International Journal of Hydrogen Energy 100 (2025) 1282–1290

Contents lists available at ScienceDirect

International Journal of Hydrogen Energy

journal homepage: www.elsevier.com/locate/he

Enhancing the power density of hydrogen release from LOHC systems by high Pt loadings on hierarchical alumina support structures

Franziska Auer [a,1], Thomas Solymosi [a,1], Chris Erhardt [a,b], Carlos Cuadrado Collados [c], Matthias Thommes [c], Peter Wasserscheid [a,b,d,*]

[a] Helmholtz Institute Erlangen-Nürnberg for Energy Technologies (IET-2), Erlangen, Germany
[b] Friedrich-Alexander-Universität Erlangen-Nürnberg (FAU), Lehrstuhl für Chemische Reaktionstechnik, Erlangen, Germany
[c] Friedrich-Alexander-Universität Erlangen-Nürnberg (FAU), Lehrstuhl für Thermische Verfahrenstechnik, Erlangen, Germany
[d] Forschungszentrum Jülich GmbH, Institute for a Sustainable Hydrogen Economy (INW), Jülich, Germany

ARTICLE INFO

Handling Editor: Prof. A.B. Basile

Keywords:
LOHC
Dehydrogenation
Space-time-yield
Power-density
Reactor
Catalyst

ABSTRACT

In this contribution, a step change in the power density of hydrogen release from LOHC systems is presented. This could be achieved by the use of hierarchical alumina supports in combination with high Pt loadings. Here, a demonstration was carried out for the catalytic dehydrogenation of perhydro dibenzyltoluene (H18-DBT). In the course of our study, different alumina support materials were characterized and loaded with 0.3, 0.6, 0.9 and 1.2 $wt\%_{Pt}$, respectively. It was found that a specific bimodal pore structure with a large pore volume in both, the mesoporous range between 10 and 25 nm and the macroporous range between 500 and 1000 nm, enabled high Pt-based productivities even at Pt loadings, four times higher than that of the current technical standard. This gives access to a substantially improved volumetric power density of the respective catalyst. In batch dehydrogenation experiments with a 1.5 mm pellet and a Pt loading of 0.9 $wt\%_{Pt}$, a doubling of volumetric power density could be achieved compared to the technical 0.3 $wt\%_{Pt}$ standard material (Clariant, Elemax D102). Our analytical work elucidated that this highly relevant increase can be related to a faster mass transfer resulting from the special pore structure of the catalyst support and to a better Pt distribution on the support resulting in a thinner egg-shell layer. Using the optimized catalyst materials in continuous fixed-bed dehydrogenation experiments higher gas hold-up in the reactor and dewetting of the catalyst surface become additional aspects that influence the overall observed catalyst performance.

1. Introduction

In the future carbon-neutral energy system, hydrogen and hydrogen-derived compounds represent important vectors for energy storage and transport [1–3]. Liquid Organic Hydrogen Carrier (LOHC) systems enable the chemical binding of hydrogen at energy-rich locations and times, storage and transport at ambient conditions using existing fuel infrastructure and release at locations and times of energy or hydrogen need [4,5]. Consequently, LOHC systems offer a practical and rapid-to-implement solution for energy and hydrogen transportation [6–10] and storage of large amounts of energy over extended times [11–13] (e.g. several days to seasonal storage). For example, the LOHC system dibenzyltoluene (H0-DBT)/perhydro dibenzyltoluene (H18-DBT) that is applied in this work provides a hydrogen storage capacity of 6.2 wt% while its physico-chemical properties are similar to diesel fuel [14].

The future technical use of LOHC systems will rely heavily on techno-economic considerations for specific use cases [6–8,15–20]. Important aspects are the hydrogen quantity and quality in demand, the transport distance, and the availability of waste heat at the location of hydrogen release [6,20,21]. A central element of the capital cost calculations for a hydrogen release unit from LOHC systems is the dehydrogenation reactor that includes the dehydrogenation catalyst. The latter consists of the support material and the active precious metal [8,10,16]. In order to reduce the costs of the reactor, it is highly attractive to increase its volumetric power density, i.e. the space-time-yield (STY) of the respective dehydrogenation reaction by an improved catalyst performance and by optimized heat and mass transport properties of the

* Corresponding author. Cauerstr. 1, 91058, Erlangen, Germany.
E-mail address: p.wasserscheid@fz-juelich.de (P. Wasserscheid).
[1] Both authors contributed equally to this work.

https://doi.org/10.1016/j.ijhydene.2024.12.155
Received 10 October 2024; Received in revised form 18 November 2024; Accepted 9 December 2024
Available online 30 December 2024

reaction system [22]. Such improvement results in a larger amount of released hydrogen for a given reactor volume or in a smaller reactor for a given hydrogen output. It is noteworthy, that a strongly increased STY may give access to application fields that have been not feasible beforehand. In particular, in the field of heavy-duty mobility applications, a higher STY may enable to meet the power demand of a given application in the restricted volume available on-board of the respective vehicle [23–26].

There are various methods to increase the STY of a dehydrogenation reactor. The most obvious methods are increasing the reaction rate by operational parameter adjustments (i.e. higher temperature, higher feed flow leading to stationary operation at a higher degree of hydrogenation, DoH) [27,28], reactor modifications (i.e. optimized heat transport [29–31], better pre-heating or use of evaporated LOHC [32,33]), and catalyst optimization (i.e. selective poisoning [34–36], adjustment of optimal catalyst nanoparticle size [36,37]). Note, that the operating temperature is limited by the chemical stability of the LOHC system [38], and the feed flow rate determines the trade-off between hydrogen output and utilization of the full LOHC storage capacity [39,40]. In terms of catalyst optimization, extensive research has been dedicated to new materials that increase productivity at given reaction conditions [34,41–44]. Another approach to enhance STY is increasing the active metal loading of the catalyst. If at higher loadings the Pt-based productivity is maintained, the reactor volume could be reduced without reducing the hydrogen output.

This study is dedicated to realizing this particular approach through a variation of the support material. Our working hypothesis is that an optimized hierarchical support material can enable higher Pt-loadings without a reduction of the Pt-based productivity and thus a significant increase in STY for the hydrogen release reaction. We chose the dehydrogenation of perhydro dibenzyltoluene (H18-DBT) as a test reaction because it enables batch screening at high temperature (310 °C) and ambient pressure without evaporation [45]. In order to obtain STY values under steady-state conditions, the best performing catalyst materials were also tested in a continuous dehydrogenation setup.

2. Experimental

2.1. Support materials and catalyst synthesis

Four different alumina support materials were kindly provided by Saint Gobain NorPro (SA51161, SA31132 (3.0 and 1.5 mm), SA31145) [46]. The supports were all in pelletized form with a diameter around 3.0 mm/1.5 mm and had a bimodal pore size distribution. Details on textural properties can be found in the results section. On the basis of these support materials, egg-shell catalysts were synthesized by wet impregnation with platinum sulfite acid solution (15.3 wt% Pt, abcr GmbH). The precursor solution was diluted with water to a Pt mass concentration of 0.05 wt% before the addition of the amount of support necessary to reach the desired platinum loading. Complete evaporation of the solvent was achieved in a rotary evaporator with a bath temperature of 50 °C and a stepwise pressure reduction to 6 kPa. After keeping it in a drying oven at 60 °C over night, the catalyst was reduced in a tubular furnace at 440 °C for 2 h by a hydrogen containing gas flow (10% H_2 in N_2). For comparison, a reference catalyst was prepared following the same procedure as described above, using a spherical alumina support material with similar properties to the commercial Elemax D102 catalyst [47].

2.2. Material characterization

The specific surface area of the support materials was determined by means of nitrogen physisorption. After degassing at 250 °C and 1 Pa, the measurements were performed in a Tristar II Plus (Micromeritics). The BET method was used in a relative pressure range from 0.05 to 0.35 to calculate the specific surface area. As the materials under investigation exhibit a bimodal pore size distribution in the meso- and macropore range, mercury intrusion porosimetry was used to assess further textural properties. The analysis was conducted in a Pascal 440 porosimeter (Thermo Electron Corporation) up to a pressure of 400 MPa. The samples were also dried and degassed before the measurement. Additionally and to characterize the pore structure in more detail, high resolution gas adsorption measurements were performed on a commercial Autosorb iQ automatic volumetric adsorption analyzer from Quantachrome (Boynton Beach, FL, USA) equipped with 1, 10 and 1000 Torr transducers. Argon at 87 K was used as adsorptive (Ar 6.0 purchased from Air-Liquide). Prior to the sorption measurements, alumina materials were outgassed at 200 °C for 12 h under high vacuum. Detailed mercury intrusion and extrusion experiments on the evaluated materials were performed over a wide range of pressures starting from vacuum to over 400 MPa using a Quantachrome Poremaster 60 instrument.

The platinum loading of the prepared catalysts was checked by inductively coupled plasma optical emission spectroscopy (ICP-OES), using a Ciros CCD device from Spectro Analytical Instruments GmbH. For the analysis, the solid samples were digested with the help of concentrated acids (3:1:1 HCl:HNO_3:HF) and microwaves. Unless stated otherwise, the desired platinum loading was reached in all cases within measurement accuracy. To evaluate the platinum particle sizes and size distributions of the catalyst on the different supports, high-resolution transmission electron microscopy (HR-TEM) was used. Sample preparation involved scraping and grinding the outer platinum-containing layer of the catalysts, dispersing the resulting powder in an isopropanol-ethanol mixture and applying it to a copper grid with lacey carbon coating (Plano GmbH). 200 to 300 particles from different TEM images were analyzed with the open-source platform Fiji [48]. The thickness of the platinum egg-shell layer of the catalysts was determined using a Leica M125C microscope.

2.3. Catalytic testing

The catalysts were initially screened in a batch dehydrogenation setup (see Fig. 1, left). For each experiment, 19.17 g of H18-DBT were added to a three-necked flask and a specified amount of catalyst was placed in the catalyst feeder to allow for a molar ratio of Pt:H18-DBT of 1:2000. The setup was purged with argon and hydrogen for 10 min each, then heated to 310 °C while maintaining a stirrer speed of 500 rpm. The catalyst was added slowly to the pre-heated H18-DBT over a period of 5 min, ensuring that the temperature remained constant. Therefore, only data obtained after 5 min and above 25% degree of dehydrogenation (DoD, see eq. (1)) were considered. Hydrogen released from the reaction was analyzed using a GSM-A mass flow meter (MFM, Vögtlin Instruments GmbH). Liquid samples were taken at 10, 15, 25, 40, 60, 90 and 120 min after the addition of the first catalyst pellets.

The most promising catalysts (SA31132 – 3.0 mm 0.6 $wt\%_{Pt}$, SA31132 – 1.5 mm 0.9 $wt\%_{Pt}$) and the reference catalyst (0.3 $wt\%_{Pt}$) were also tested in a continuous dehydrogenation setup. The reactor tube ($d_i = 10$ mm, $l = 150$ mm) was filled with the catalyst up to a height of 122 mm ($V_{cat} = 9.6$ mL) and the remaining 23 mm were filled with glass beads to avoid cooling by back-mixed liquid. After assembly, the setup was initially purged with argon and hydrogen for 15 min each and then heated to 300 °C jacket temperature. The internal temperature of the reactor at the center was monitored using a type K thermocouple. The conditions at the different operating steps are listed in Table 1. The released hydrogen was gravimetrically separated from the liquid, cooled down, purified using an activated carbon filter and quantified by an MFM GSM-A (Vögtlin Instruments GmbH). The dehydrogenated LOHC species passed through the siphon into the product tank. Liquid samples were taken at the end of each operating step to confirm the MFM measurements and deviations were always smaller than 5%.

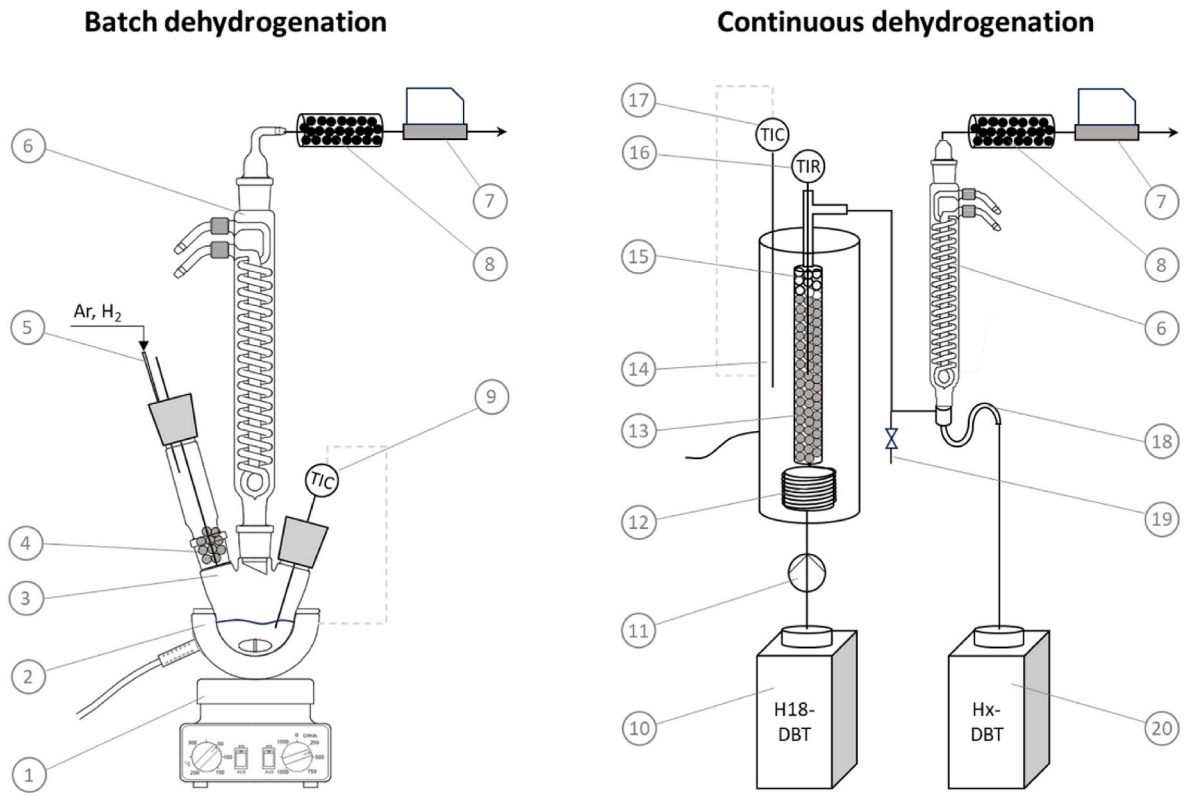

Fig. 1. Experimental setups for batch (left) and continuous (right) dehydrogenation. (1) Stirrer, (2) heating mantle, (3) three-necked flask with H18-DBT and stirring bar, (4) catalyst in addition device, (5) gas inlet for argon and hydrogen, (6) cooler, (7) mass flow meter (MFM), (8) activated carbon filter, (9) thermocouple controlling the heating jacket, (10) feed tank with H18-DBT, (11) pump, (12) preheating coil, (13) fixed bed reactor with catalyst, (14) heating jacket, (15) glass beads, (16) thermocouple in reactor middle, (17) thermocouple controlling the heating jacket, (18) siphon for gas/liquid separation, (19) liquid sampling, (20) product tank.

Table 1
Operating conditions of the continuous dehydrogenation experiments for each catalyst.

Operating step	Heating jacket temperature in °C	Feed in g/min	Duration in h
Flooding	300	5,4	0.1
Day 1–1	300	0,5	1.5
Day 1–2	310	0,5	1
Day 1–3	310	1,5	1
Day 1–4	310	3,0	1
Day 1–5	So that $TIR_{catalyst} \approx 310$ °C	0,5	1
Over night	310	0,5	15–18
Day 2–1	300	0,5	1
Day 2–2	310	1,5	1
Day 2–3	310	3,0	1
Day 2–4	So that $TIR_{catalyst} \approx 310$ °C	0,5	1

2.4. LOHC product analysis

The liquid Hx-DBT samples were characterized regarding the DoD via ^{1}H NMR as previously described [30,49]. For the evaluation of the corresponding spectra the software ACD Spectrus Processor was used.

2.5. Calculations

Besides liquid phase analysis via NMR, the DoD was calculated via the continuous gas phase analysis by a mass flow meter according to eq. (1) with $\dot{V}_{N,H_2}$ being the measured volumetric hydrogen stream and $n_{H18-DBT}$ being the molar amount of H18-DBT used in the batch experiment. Both methods for DoD analysis (liquid and gas phase) agreed very well and deviations were always below 5%.

$$DoD(t) = DoD_0 + \frac{\int_0^t \dot{V}_{N,H_2} dt \bullet 0,0899 \frac{g_{H2}}{L_{N,H2}}}{n_{H18-DBT} \bullet 18,14 \frac{g_{H2}}{mol_{H18-DBT}}} \quad (1)$$

For the continuous experiments, the DoD was calculated according to eq. (2) with $\dot{n}_{H18-DBT}$ being the molar feed of H18-DBT.

$$DoD = DoD_0 + \frac{\dot{V}_{N,H_2}(t) \bullet 0,0899 \frac{g_{H2}}{L_{N,H2}}}{\dot{n}_{H18-DBT} \bullet 18,14 \frac{g_{H2}}{mol_{H18-DBT}}} \quad (2)$$

The mass-related productivity P_m was calculated according to eq. (3) with m_{Pt} being the platinum mass used in the experiment.

$$P_m(t) = \frac{\dot{V}_{N,H_2}(t) \bullet 0,0899 \frac{g_{H2}}{L_{N,H2}}}{m_{Pt}} \quad (3)$$

To compare the different catalysts in the batch experiment, the mean productivity $P_{30\%-40\%}$ between a DoD of 30% and 40% was calculated.

The volumetric productivity P_{vol}, which describes the productivity related to the packing volume of the catalyst, was calculated according to eq. (4) with ρ_{cat} being the packing density of the catalyst and $w_{Pt,cat}$ being the weight loading of platinum on the catalyst. For continuous experiments P_{vol} equals the STY.

$$P_{vol} = P_m \bullet w_{Pt,cat} \bullet \rho_{cat} \quad (4)$$

Since the support materials have different packing densities, we also considered the platinum density in the packing volume of the used catalyst ρ_{Pt} for a better comparison according to eq. (5).

$$\rho_{Pt} = w_{Pt,cat} \bullet \rho_{cat} \quad (5)$$

3. Results and discussion

Different characteristic properties of the applied catalyst support materials were determined by nitrogen physisorption, mercury intrusion and weighing of a defined packing volume. The results are shown in Table 2 in comparison with the values from the supplier data sheet. The corresponding sorption isotherms and pore size distributions can be found in the ESI.

Overall, the measured data are in reasonable agreement with the supplier information [46] and the values lie in the same orders of magnitude. Deviations can be attributed to batch fluctuations during production and measurement accuracy. From the data an inverse correlation between specific surface area and pore size can be seen. To evaluate the influence of these parameters on dehydrogenation activity, different catalysts were prepared on the basis of the support materials and tested in the batch dehydrogenation of H18-DBT. The calculated mass-based productivities of the catalysts A, B and C with the corresponding support materials are shown in Fig. 2 together with their characteristic properties. The reference line indicates the productivity of the reference catalyst equally to the commercial material.

From the graphical representation in Fig. 2, a maximum in mass-related productivity can be seen for catalyst B. The determined value of 4.3 g_{H2} g_{Pt} min^{-1} corresponds to a 12% increase in comparison to the technical reference material. As the observable dehydrogenation activity is the result of a complex interplay of different catalyst properties, catalyst B seems to feature the most advantageous combination of these properties among the tested catalyst samples. An intermediate surface area of 69 m^2 g^{-1} enables a good dispersion of Pt on the catalyst support (Fig. 3). Accordingly, the mean Pt particle diameter is found to be 1.00 nm and is thus significantly smaller than the one of catalyst A (2.04 nm) with a specific surface area of only 6 m^2 g^{-1}. Furthermore, the particle size distribution is significantly broader for the latter (see ESI). In contrast, catalyst C with an even larger surface area of 80 m^2 g^{-1} does not show a smaller Pt particle size nor a higher productivity compared to catalyst B. This leads to the conclusion that a sufficiently large surface area is needed to obtain a good Pt dispersion but a further increase beyond this value does not lead to further improvement. Conversely, a larger specific surface area is associated with a smaller pore size which can lead to mass transport limitations due to the relatively large LOHC-molecules [35,36]. Besides the pore dimensions, the thickness of the platinum egg-shell layer has also been found to influence mass transport limitations [50]. The catalyst layer-thickness is again influenced by the specific surface area of the support. A larger surface area leads to thinner platinum egg-shell layers, as can be seen from Fig. 3. There is a certain difference between the measured values for catalyst B (101 µm) and C (49 µm), while the small surface area of catalyst A is associated with a full impregnation of the catalyst pellet and therefore a stronger influence of mass transport limitations.

Based on these results, catalyst B was chosen for further investigations. In addition to the 3.0 mm pellet, a smaller one with 1.5 mm diameter was also tested. The aim of this additional catalyst pellet size was to provide a larger outer surface area to improve mass transport and to achieve a higher packing density and therefore a higher Pt amount in the reactor. As the power density of LOHC dehydrogenation reactors depends on the amount and utilization of platinum metal in the reactor, a Pt loading variation was carried out. Catalysts with Pt loadings between 0.3 and 0.9 $wt\%_{Pt}$ were synthesized and tested in the batch dehydrogenation of H18-DBT. The Pt loadings and the catalyst productivities were normalized to the catalyst packing volume to enable a theoretical transfer of the results to continuous fixed-bed reactors. The results are shown in Fig. 4.

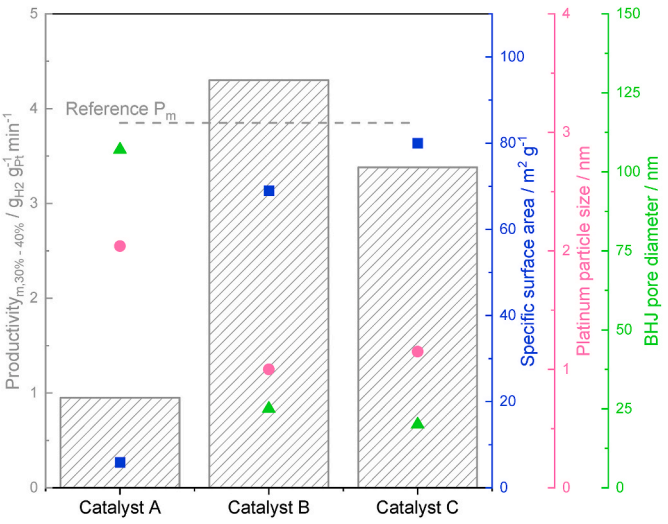

Fig. 2. Mass-related productivities in the batch dehydrogenation of H18-DBT and characteristic properties of the catalysts based on the support materials A, B and C, 3.0 mm pellets. Experimental conditions: T = 583.15 K, p = 1 bar (a), n(H18-DBT) = 0.066 mol, n(Pt):n(H18-DBT) = 1:2000, $w_{Pt,cat}$ = 0.3 $wt\%_{Pt}$.

Interestingly, different trends can be observed for the catalysts based on the reference support material and the support material B with increasing Pt loading. Concentrating on the 3.0 mm version of catalyst B first, a doubling of the platinum loading from 0.3 to 0.6 $wt\%_{Pt}$, which corresponds to platinum densities of 1.8 and 3.6 g_{Pt} L_{cat}^{-1}, respectively, is accompanied by an increase in volumetric productivity by 61%, whereas a decrease by 11% was found for the reference. But no further improvement was achieved when the catalyst loading was increased to 0.9 $wt\%_{Pt}$ for catalyst B, 3.0 mm. To explain the different behaviour of the reference and catalyst B, factors that influence the effectiveness of the Pt utilization in the different catalysts have to be considered. In this regard, the Pt dispersion and the Pt distribution within the catalyst pellet, i.e. the thickness of the egg-shell layer, are of special interest. It can be assumed that with increasing Pt loading, especially in combination with a low specific surface area, larger Pt particles or thicker egg-shell layers are formed which both would result in a lower Pt-based catalyst productivity. To verify this assumption, TEM and light microscope images of the two catalysts with loadings of 0.3 and 0.6 $wt\%_{Pt}$ were compared (Fig. 5).

From the TEM images an increase in Pt particle size can be seen for both catalysts with higher Pt loading. For the reference material the mean particle diameter changes from 1.28 to 1.48 nm, for catalyst B a

Table 2
Characteristic properties of different catalyst support materials; comparison of supplier information and measured data.

	Material A SA51161		Material B SA31132		Material C SA31145	
	catalogue	measured	catalogue	measured	catalogue	measured
Specific surface area (m^2 g^{-1})	4.5	5.9[a]	55	69[a]	75	80[a]
Pore size (nm)	100/11,000	107/20,000[b]	25/550	16/740[b]	20/230	17/270[b]
Packing density (kg L^{-1})	0.96	0.99[c]	0.55	0.60[c]	0.66	0.70[c]

[a] N_2 physisorption.
[b] Hg porosimetry.
[c] Weighing of defined packing volume.

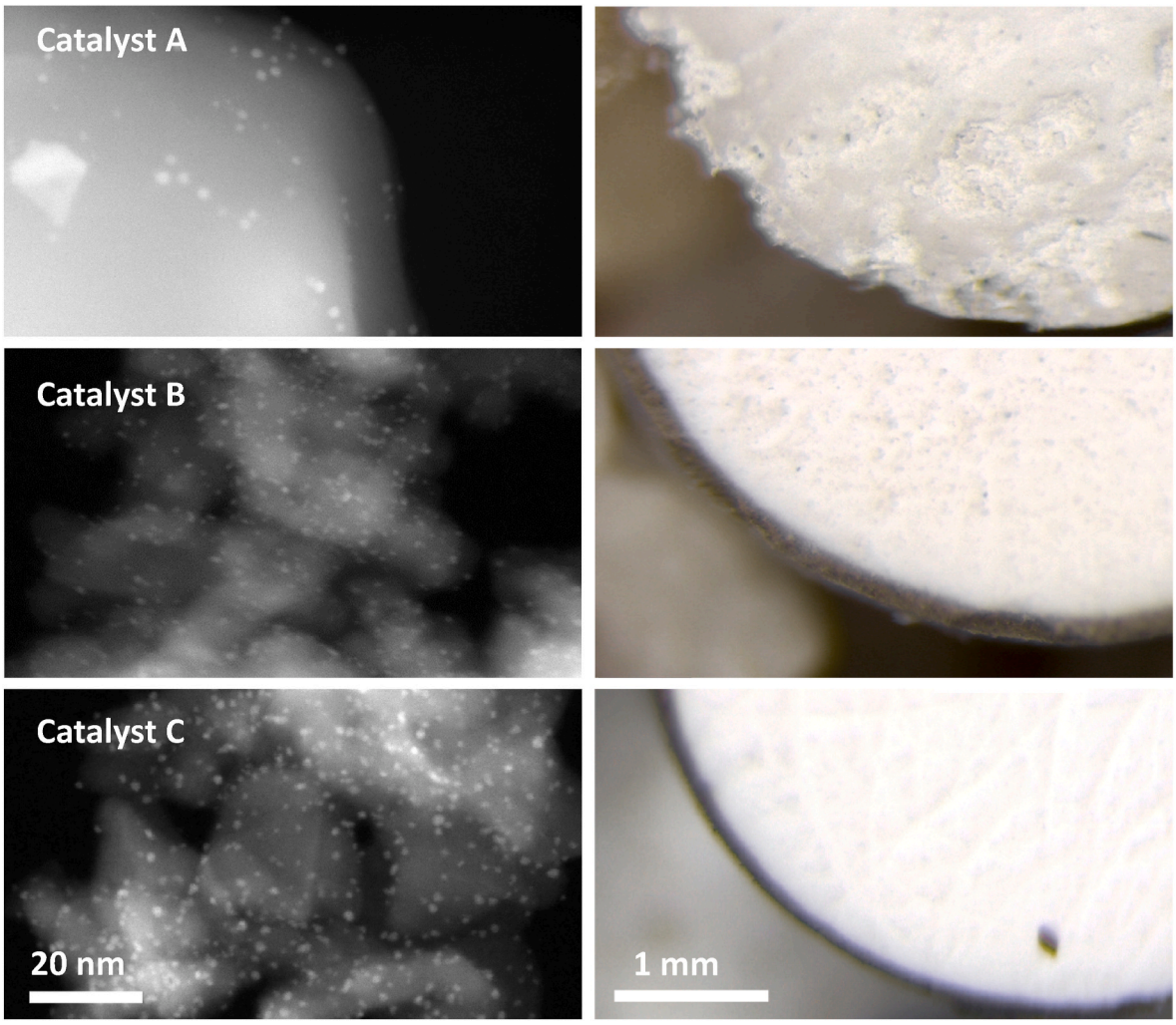

Fig. 3. TEM images of Pt-nanoparticles (left) and light microscope images of cross-sections with visible platinum egg-shell layer (right) of catalysts A, B and C.

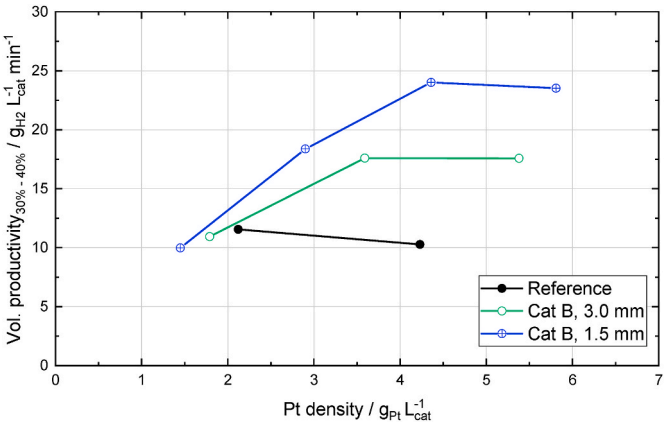

Fig. 4. Volumetric productivity between 30% and 40% DoD in the batch dehydrogenation of H18-DBT over platinum density of catalysts with different loadings and based on reference and support material B, 1.5 and 3 mm pellets. Experimental conditions: T = 583.15 K, p = 1 bar(a), n(H18-DBT) = 0.066 mol, n(Pt):n(H18-DBT) = 1:2000, $w_{Pt,cat}$ = 0.3, 0.6, 0.9, 1.2 $wt\%_{Pt}$.

change from 1.00 to 1.33 nm is observed. Since the increase in particle size with increasing Pt loading is consistent for both catalyst types, this cannot explain the observed difference in relative catalytic activity between the different loadings for the two different supports. Regarding the Pt egg-shell thickness, an increase from 215 to 268 μm was determined for the reference catalysts whereas almost no change (101 vs. 104 μm) was found for catalyst B. Consequently, the thickening of the Pt egg-shell layer with increasing Pt loading could explain the productivity drop in case of the reference catalyst in comparison to catalyst B. A reason for this could be the larger specific surface area and the bimodal pore structure of catalyst B. To validate this assumption, high-resolution gas adsorption and mercury intrusion/extrusion measurements were performed with the corresponding support materials. The so-determined pore size distributions are shown in Fig. 6.

For both support materials, no pores in the micropore range (<2 nm) can be observed. These would also not be beneficial in the case of H18-DBT dehydrogenation due to the size of the molecules and the resulting mass transport limitations. Mesopores (2–50 nm), in contrast, enable a fast diffusional transport of the LOHC molecules and generate the inner surface area necessary to enable a good dispersion of the Pt nanoparticles. Astonishingly, the support material of catalyst B provides an approximately three times higher pore volume in this very beneficial pore size range. The larger mesopore volume with its inner surface area is capable of taking up a higher Pt loading without increasing the penetration depth. Furthermore, it is noticeable that support B also exhibits a higher pore volume in the macropore range (>50 nm) than the reference. Macropores can further enhance the transport of LOHC molecules and the nucleation of hydrogen gas bubbles which accelerates mass transport and therefore the microkinetic reaction rate in two ways. The described beneficial structure of the new catalyst B in comparison to

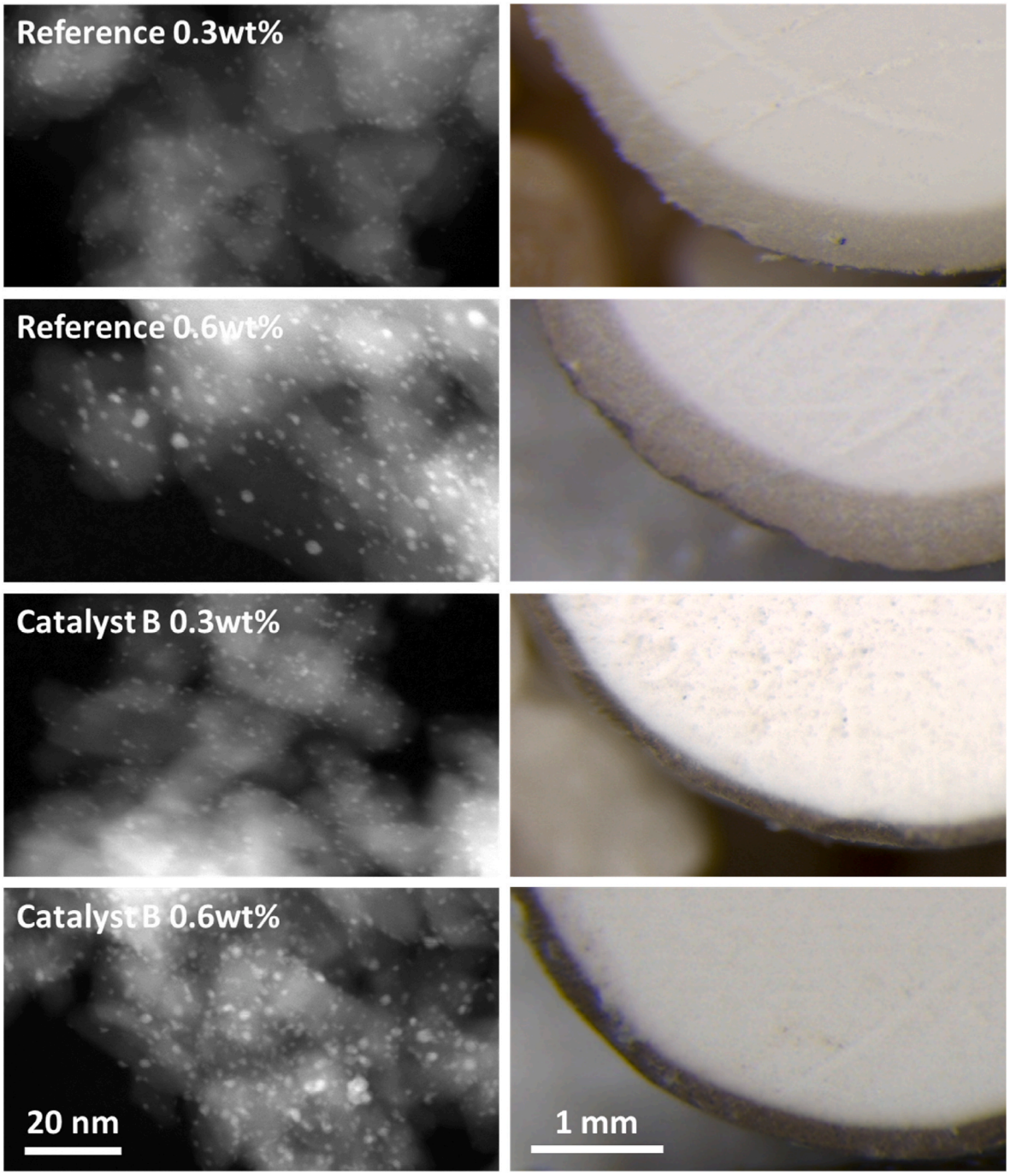

Fig. 5. TEM images of Pt-nanoparticles (left) and light microscope images of cross-sections with visible Pt egg-shell layer (right) of different catalysts based on reference and support material B and loadings of 0.3 and 0.6 $wt\%_{Pt}$.

the reference, showing the support (white), the Pt egg-shell layer (grey) and the Pt nanoparticles (black) is illustrated in Fig. 7.

Overall, the results show impressively that the high pore volume of the catalyst support material B in both the meso- and the macropore range is likely to create the prerequisite for high Pt-based productivities at enhanced Pt loadings on the support. In this way, substantially higher volume-related productivities can be achieved during hydrogen release from H18-DBT. At a Pt loading of 0.6 $wt\%_{Pt}$ a 150% increase in STY could be achieved in the batch dehydrogenation experiment using the new catalyst support with a 1.7 times higher Pt density compared to the commercial reference material.

To further improve the volumetric productivity of a support B-based dehydrogenation catalyst, smaller pellets with 1.5 mm diameter were used for catalyst preparation. The results are also shown in Fig. 4. In contrast to the 3.0 mm pellets, the 1.5 mm pellets of catalyst B show a further increase in volumetric productivity with a rise in the Pt loading from 0.6 to 0.9 $wt\%_{Pt}$. Remarkably, for the 1.5 mm pellet at a loading of 0.9 $wt\%_{Pt}$, a smaller Pt egg-shell thickness of 155 μm is reached in comparison to 170 μm for the 3 mm pellet. The left-shift of the curve for catalyst B, 1.5 mm compared to the 3.0 mm-sized material can be explained by the slightly lower packing density of the smaller pellets (0.48 kg L^{-1} vs. 0.60 kg L^{-1}). Again, an even higher loading of 1.2 $wt\%_{Pt}$ does not lead to a further improvement regarding the volumetric productivity of catalyst B, 1.5 mm. Compared to the commercial reference catalyst, the use of 1.5 mm pellets of catalyst B with a loading of 0.9 $wt\%_{Pt}$ leads to an impressive increase of the theoretical STY by 200% with

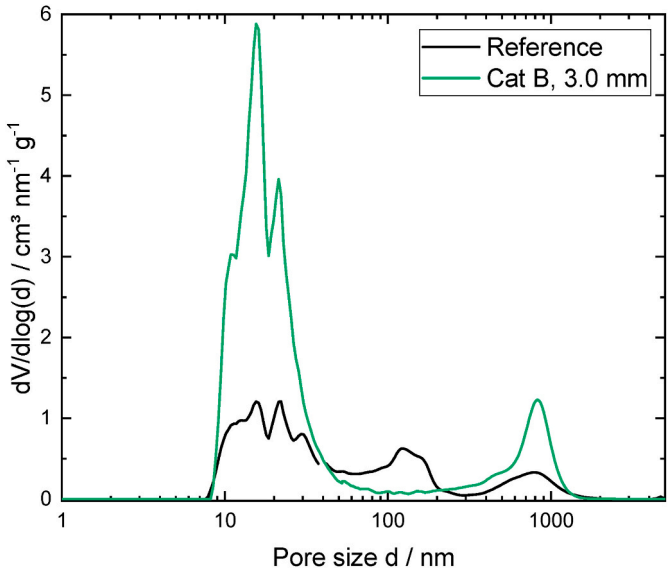

Fig. 6. Pore size distributions of the reference and catalyst B support materials derived from high-resolution Ar (87 K) gas adsorption and mercury intrusion measurements.

a doubling of the Pt density.

Besides the demonstrated advantages of the smaller pellets, a higher pressure drop for larger catalyst beds was suspected when using these smaller pellets. Therefore, we measured the pressure drop in a 70 cm long fixed bed (d_i = 28 mm) of a cold-flow setup for each support type with water and air streams comparable to the fluid flows in a potential technical dehydrogenation reactor. Although the pressure drop was significantly higher for the small pellets, all measured values were in an uncritical range below 50 mbar (see ESI for more details).

3.1. Continuous dehydrogenation

To check whether the trends derived from the batch experiments are also confirmed in continuous steady-state operation, the two most promising catalysts (Cat B, 3.0 mm 0.6 $wt\%_{Pt}$ and Cat B, 1.5 mm 0.9 $wt\%_{Pt}$) and the reference catalyst (0.3 $wt\%_{Pt}$) were tested in a small continuous fixed bed reactor setup. As the different activities of the catalysts lead to different DoDs at the same operation conditions, a variation of the feed rates was conducted to lay the foundation for a fair comparison of productivities at the same DoD at the reactor outlet. Fig. 8A shows the volumetric productivity of the catalysts after 22 h runtime at 300 °C (fully stationary operation) and different feed rates (grey lines). At high feed rates the residence time is short, the resulting DoD of the LOHC is low and the productivity is high due to a high concentration of remaining fully hydrogenated LOHC in the reactor. At a lower feed rate, the residence time increases, and consequentially the productivity decreases at higher DoDs. At a DoD of 48% the 3.0 mm 0.6 $wt\%_{Pt}$ version of catalyst B shows a 2.5 times higher productivity than the reference (3.93 vs. 1.55 $g_{H2}\ L_{cat}^{-1}\ min^{-1}$), which is even more convincing than expected from the batch experiments. Due to the different packing densities of the pellets, the catalyst bed with the 3.0 mm 0.6 $wt\%_{Pt}$ pellets of catalyst B exhibited only a 1.7 times higher platinum density than the packing of the reference catalyst. This means, that the STY of the reactor is not only linearly increased by the higher Pt-loading but also by a higher mass-related productivity.

The even higher loaded 1.5 mm 0.9 $wt\%_{Pt}$ catalyst B showed a much smaller productivity than the 3.0 mm 0.6 $wt\%_{Pt}$ catalyst under all tested reaction conditions in the continuous reactor. Although the productivity at a DoD of 48% is 1.6 times higher than for the reference catalyst, the platinum density in the reactor is 2.3 times higher (see also ESI). This means that a smaller increase in STY was achieved.

Fig. 8B shows the comparison between the batch and continuous dehydrogenation experiments at 310 °C. Note that the fixed bed reactor was set to a core temperature of 310 °C and the jacket temperature had to be set accordingly higher (7–11 °C depending on activity) due to the endothermicity of the reaction. Since the feed rate was always set to 0.5 g min^{-1}, the achieved DoD differed for the different catalysts. Therefore, we compared the productivities from batch and continuous experiments at the same DoD for each catalyst. It is known that the catalyst-based productivity in continuous operation is significantly smaller than in batch operation [28,36] due to a higher Pt:LOHC-ratio and a higher gas holdup in the continuous reactor. In direct comparison, the reference catalyst achieved 28% of the batch productivity at a DoD of 58% in continuous operation, while catalyst B, 3.0 mm 0.6 $wt\%_{Pt}$, reached 60% of the batch productivity at a DoD of 81%. Accordingly, the use of catalyst B, 3.0 mm 0.6 $wt\%_{Pt}$, not only leads to a significant increase in STY with a relatively smaller increase in platinum density, but also allows the productivity to be closer to the respective batch values (60% vs. 28% of the batch productivity). This makes the catalyst B, 3.0 mm 0.6 $wt\%_{Pt}$, highly attractive for the use in power-dense dehydrogenation reactors. Surprisingly, the 1.5 mm 0.9 $wt\%_{Pt}$ catalyst B that performed best in batch experiments, showed the largest deviation in the continuous setup and only reached 14% of its batch productivity. To explain this

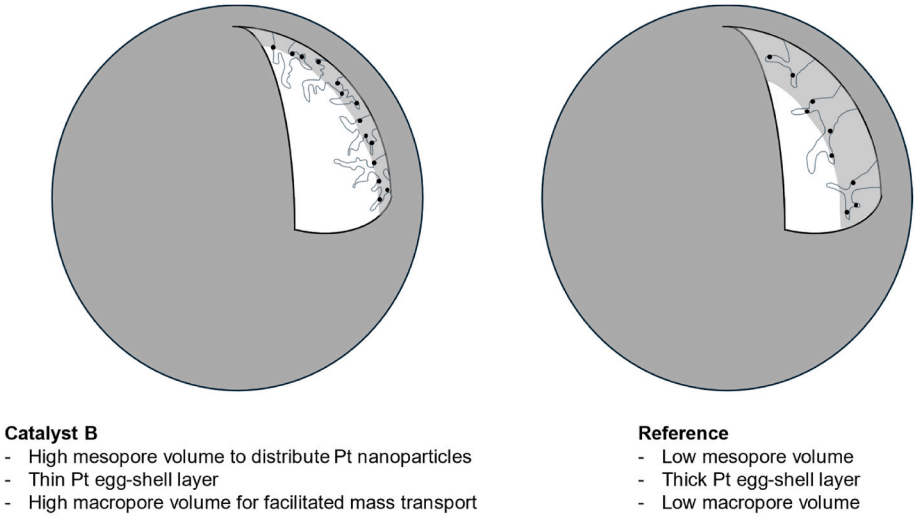

Fig. 7. Illustration of the proposed structure of the catalysts, showing the support (white), the Pt egg-shell layer (grey) and the Pt nanoparticles (black).

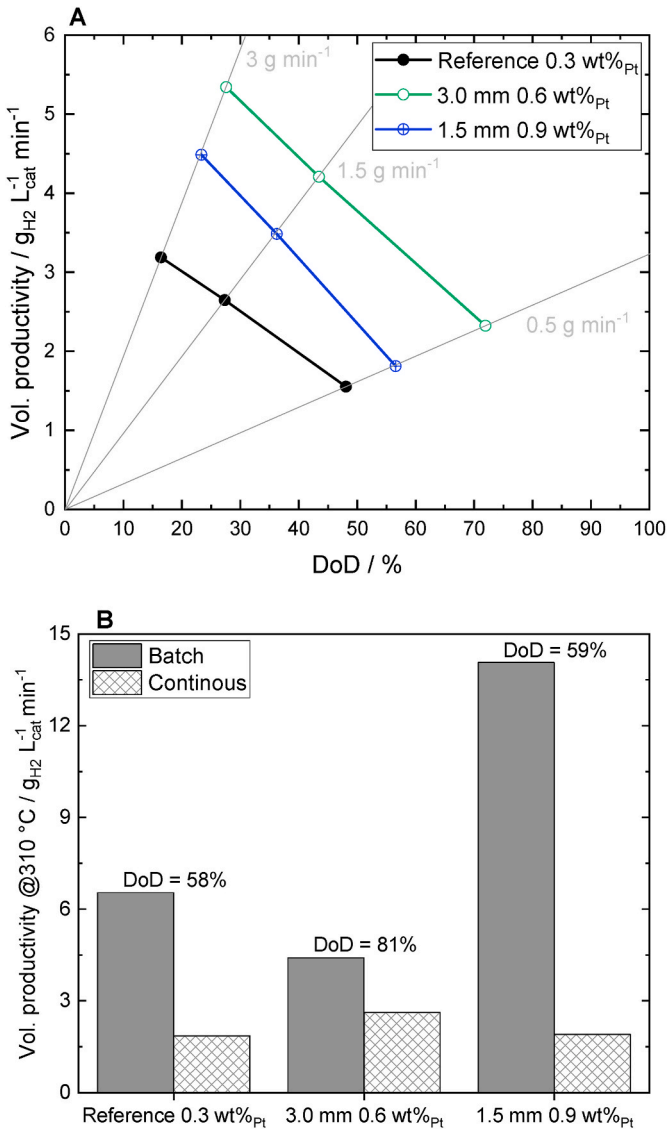

Fig. 8. (A) Volumetric productivity over DoD at different feed rates and 300 °C in the continuous dehydrogenation of H18-DBT for reference catalyst (0.3 wt%, 5.582 g), 3.0 mm catalyst B (0.6 wt%$_{Pt}$, 4.704 g) and 1.5 mm catalyst B (0.9 wt%$_{Pt}$ 4.214 g); (B) comparison of volumetric productivity at 310 °C in batch and continuous (core temperature) operation mode at different DoDs.

discrepancy, we performed additional experiments in both, a transparent cold-flow setup and a glass test tube of similar dimensions as the fixed-bed reactor. Within the packing of the 1.5 mm pellets much smaller interparticle voids were observed and, as a result, more liquid was pushed out of these voids as compared to the bigger catalysts for the same gas flow (see ESI for more details). This caused a higher gas holdup in the packing leading to partial dewetting of the catalyst and, consequently, to a much lower productivity. Our results reveal important differences in catalyst testing for stirred tank and fixed-bed reactors that have to be taken into account in future catalyst performance evaluation studies. We provide catalyst stability information in the ESI. At a DoD of 48% all catalysts were tested over 22 h time-on-stream with the most active 3.0 mm 0.6 wt%$_{Pt}$ catalyst on support B showing a performance loss of only 9.4 % during this operation time, indicating very reasonable catalyst stability also at these strongly enhanced volumetric catalyst productivities. Furthermore, catalyst B shows a similar selectivity regarding the formation of high-boiling side products in comparison to the reference (see ESI for more details).

4. Conclusion

In order to explore the possibilities of using high-loaded Pt/Al_2O_3 catalysts to increase the power density of LOHC dehydrogenation reactors, three different commercially available alumina support materials with different textural properties were characterized and impregnated with 0.3 wt%$_{Pt}$. The catalyst based on a support material with intermediate specific surface area (25 m^2 g^{-1}) and pore size (bimodal, 25/550 nm) reached the highest productivity among the tested catalysts in batch dehydrogenation experiments with H18-DBT. These new catalyst materials even exceeded the productivity of the commercial reference catalyst by 12%. The best material (based on support B) – in two pellet sizes of 3.0 and 1.5 mm diameter – was then loaded with higher amounts of Pt, namely 0.6, 0.9 and 1.2 wt%$_{Pt}$. Batch dehydrogenation experiments revealed that the catalysts based on this optimized support material enable significantly higher volume-based productivities or STYs compared to the commercial reference. With a 3.0 mm pellet of the optimized support and a loading of 0.6 wt%$_{Pt}$ a 150% increase in volume-based productivity could be achieved at a 1.7 times higher Pt density compared to the commercial reference. With a 1.5 mm pellet an even higher loading of 0.9 wt%$_{Pt}$, associated with an impressive increase of the volumetric productivity by 200%, could be reached.

The reason for the improved performance of the new high-loaded catalysts was found in a very beneficial bimodal pore structure of support B with a large pore volume in both, the mesoporous range between 10 and 25 nm and the macroporous range between 500 and 1000 nm. The high pore volume in the mesoporous range thereby enables a good Pt dispersion within the catalyst pellet, linked to a reduced Pt egg-shell thickness. The larger macropore volume facilitates mass transport and bubble nucleation. A larger outer surface of the catalyst area in case of the 1.5 mm pellets contributes to a reduction of mass transport limitations due to a resulting thinner Pt-containing eggshell.

Continuous dehydrogenation experiments with H18-DBT confirmed the obtained results, but hint at additional influencing factors that have to be considered in packed-bed reactors. At a DoD of 48% the 3.0 mm 0.6 wt%$_{Pt}$ catalyst B showed a 2.5 times higher productivity than the reference (3.93 vs. 1.55 g_{H2} L^{-1}_{cat} min^{-1}), whereas the 1.5 mm 0.9 wt%$_{Pt}$ version performed worse than expected, with a productivity only 1.6 times higher than the reference. While the reduced pellet sizes showed only a negligible pressure drop over the catalyst packing of below 50 mbar in cold flow experiments, the 1.5 mm catalyst poses the challenge of reduced void space, higher gas hold-up and strong dewetting of the catalyst. These issues reduce the LOHC contact with the catalyst and the heat supply to the endothermic dehydrogenation reaction.

Our contribution reveals for the first time a very significant influence of the support's pore structure on the reachable volumetric power density in LOHC dehydrogenation reactors. This will pave the way for specific catalyst optimization strategies for use cases where volumetric power density of the hydrogen release reaction is a performance critical aspect, such as e.g. in the case of hydrogen release from LOHC systems onboard of heavy-duty vehicles [51].

CRediT authorship contribution statement

Franziska Auer: Writing – original draft, Visualization, Validation, Supervision, Project administration, Methodology, Investigation, Formal analysis, Data curation, Conceptualization. **Thomas Solymosi:** Writing – original draft, Visualization, Validation, Supervision, Project administration, Methodology, Investigation, Formal analysis, Data curation, Conceptualization. **Chris Erhardt:** Writing – review & editing, Investigation, Formal analysis, Data curation, Conceptualization. **Carlos Cuadrado Collados:** Writing – review & editing, Methodology, Investigation, Formal analysis, Data curation, Conceptualization. **Matthias Thommes:** Writing – review & editing, Validation, Supervision, Resources, Project administration, Funding acquisition, Conceptualization. **Peter Wasserscheid:** Writing – review & editing, Validation,

Supervision, Resources, Project administration, Funding acquisition, Conceptualization.

Declaration of competing interest

The authors declare the following financial interests/personal relationships which may be considered as potential competing interests: Peter Wasserscheid is founder and minority shareholder of the company Hydrogenious LOHC technologies (www.hydrogenious.net) that offers commercially hydrogen storage systems based on the LOHC technology. There is no conflict of interest to declare with regard to the specific scientific results reported in this paper.

Acknowledgements

The authors would like to thank Saint Gobain Norpro for the kind provision of samples of the different alumina support materials. Special thanks goes to Dr. Michael Pabel for fruitful discussions. The authors further acknowledge financial support by the Bavarian Ministry of Economic Affairs, Regional Development and Energy through the project “Emissionsfreier und stark emissionsreduzierter Bahnverkehr auf nicht-elektrifizierten Strecken”.

Appendix A. Supplementary data

Supplementary data to this article can be found online at https://doi.org/10.1016/j.ijhydene.2024.12.155.

References

[1] Hydrogen Council;. Hydrogen scaling up: a sustainable pathway for the global energy transition. Report 2017.
[2] Züttel A, Remhof A, Borgschulte A, Friedrichs O. Phil Trans Math Phys Eng Sci 2010;368:3329.
[3] Arsad AZ, Hannan MA, Al-Shetwi AQ, Mansur M, Muttaqi KM, Dong ZY, Blaabjerg F. Int J Hydrogen Energy 2022;47:17285.
[4] Brückner N, Obesser K, Bösmann A, Teichmann D, Arlt W, Dungs J, Wasserscheid P. ChemSusChem 2014;7:229.
[5] Preuster P, Papp C, Wasserscheid P. Accounts Chem Res 2017;50:74.
[6] Hurskainen M, Ihonen J. Int J Hydrogen Energy 2020;45:32098.
[7] Niermann M, Timmerberg S, Drünert S, Kaltschmitt M. Renew Sustain Energy Rev 2021;135:110171.
[8] Abdin Z, Tang C, Liu Y, Catchpole K. iScience 2021;24.
[9] Hurskainen M. Liquid organic hydrogen carriers (LOHC): Concept evaluation and techno-economics. Research report 2019.
[10] Teichmann D, Arlt W, Wasserscheid P. Int J Hydrogen Energy 2012;37:18118.
[11] Niermann M, Beckendorff A, Kaltschmitt M, Bonhoff K. Int J Hydrogen Energy 2019;44:6631.
[12] Reuß M, Grube T, Robinius M, Preuster P, Wasserscheid P, Stolten D. Appl Energy 2017;200:290.
[13] El-Taweel NA, Khani H, Farag HEZ. IEEE Trans Sustain Energy 2020;11:1381.
[14] Preuster P, Alekseev A, Wasserscheid P. Annu Rev Chem Biomol Eng 2017;8:445.
[15] Byun M, Lee A, Cheon S, Kim H, Lim H. Energy Convers Manag 2022;268:116001.
[16] Brigljević B, Byun M, Lim H. Appl Energy 2020;274:115314.
[17] Uhrig F, Kadar J, Müller K. Energy Sci Eng 2020;8:2044.
[18] Di Lullo G, Giwa T, Okunlola A, Davis M, Mehedi T, Oni AO, Kumar A. Int J Hydrogen Energy 2022;47:35293.
[19] Rao N, Lele AK, Patwardhan AW. Int J Hydrogen Energy 2022;47:28530.
[20] Eypasch M, Schimpe M, Kanwar A, Hartmann T, Herzog S, Frank T, Hamacher T. Appl Energy 2017;185:320.
[21] Li L, Vellayani Aravind P, Woudstra T, van den Broek M. Energy Convers Manag 2023;276:116555.
[22] Perreault P, van Hoecke L, Pourfallah H, Kummamuru NB, Boruntea C-R, Preuster P. Curr Opin Green Sustainable Chem 2023;41:100836.
[23] Zenner M, Teichmann D, Di Pierro M, Dungs J. ATZ - Automobiltechnische Zeitschrift 2012;114:940.
[24] Schlapbach L. Nature 2009;460:809.
[25] Wieland S, Baumann F, Starz KA. New powerful catalysts for autothermal reforming of hydrocarbons and water-gas shift reaction for on-board hydrogen generation in automotive pemfc applications. 2001.
[26] Qureshi F, Yusuf M, Ibrahim H, Kamyab H, Chelliapan S, Pham CQ, Vo D-VN. Environ Res 2023.
[27] Geißelbrecht M. Prozessintensivierung für die Wasserstofffreisetzung aus flüssigen organischen Wasserstoffträgern. Friedrich-Alexander-Universität Erlangen-Nürnberg; 2021.
[28] Solymosi T. Entwicklung eines katalytisch aktivierten Plattenwärmetauschers zur Dehydrierung von Perhydro-Dibenzyltoluol. Friedrich-Alexander-Universität Erlangen-Nürnberg; 2021.
[29] Heublein N, Stelzner M, Sattelmayer T. Int J Hydrogen Energy 2020;45:24902.
[30] Solymosi T, Auer F, Dürr S, Preuster P, Wasserscheid P. Int J Hydrogen Energy 2021;46:34797.
[31] Nathrath P, Baier B, Raed Ramzi Y, Schühle P, Wasserscheid P. Chem Ing Tech 2022;94:1331.
[32] Geißelbrecht M, Mrusek S, Müller K, Preuster P, Bösmann A, Wasserscheid P. Energy Environ Sci 2020;13:3119.
[33] Rüde T, Lu Y, Anschütz L, Blasius M, Wolf M, Preuster P, Wasserscheid P, Geißelbrecht M. Energy Technol 2023;11:2201366.
[34] Auer F, Blaumeiser D, Bauer T, Bösmann A, Szesni N, Libuda J, Wasserscheid P. Catal Sci Technol 2019;9:3537.
[35] Seidel A. Entwicklung eines technischen Platin-Trägerkatalysators zur Dehydrierung von Perhydro-Dibenzyltoluol. Friedrich-Alexander-Universität Erlangen-Nürnberg; 2019.
[36] Auer F. Katalysatorentwicklung für die Dehydrierung von Perhydro-Dibenzyltoluol. Friedrich-Alexander-Universität Erlangen-Nürnberg; 2020.
[37] Mahayni Y, Maurer L, Auer F, Hutzler A, Wasserscheid P, Wolf M. Catal Sci Technol 2024;14:5464.
[38] Modisha P, Bessarabov D. Sustain Energy Fuels 2020;4:4662.
[39] Geiling J. Dynamische Freisetzung von Energie mit einem System aus PEM-Brennstoffzelle und LOHC-basierter Wasserstoffspeicherung. Friedrich-Alexander-Universität Erlangen-Nürnberg; 2022.
[40] Geiling J, Wagner L, Auer F, Ortner F, Nuß A, Seyfried R, Stammberger F, Steinberger M, Bösmann A, Öchsner R, Wasserscheid P, Graichen K, März M, Preuster P. J Energy Storage 2023;72:108478.
[41] Auer F, Hupfer A, Bösmann A, Szesni N, Wasserscheidpeter P. Catal Sci Technol 2020;10:6669.
[42] Modisha P, Garidzirai R, Güneş H, Bozbag SE, Rommel S, Uzunlar E, Aindow M, Erkey C, Bessarabov D. Catalysts 2022;12:489.
[43] Sekine Y, Higo T. Top Catal 2021;64:470.
[44] Strauch D, Weiner P, Sarma BB, Körner A, Herzinger E, Wolf P, Zimina A, Hutzler A, Doronkin DE, Grunwaldt J-D, Wasserscheid P, Wolf M. Catal Sci Technol 2023.
[45] Dürr S, Zilm S, Geißelbrecht M, Müller K, Preuster P, Bösmann A, Wasserscheid P. Int J Hydrogen Energy 2021;46:32583.
[46] Gobain Norpro Saint. Catalyst Carriers Typic. Propert.: Brochure 2024.
[47] Clariant, EleMax® Series, https://www.clariant.com/de/Solutions/Products/2019/05/21/15/19/EleMax-Series.
[48] Schindelin J, Arganda-Carreras I, Frise E, Kaynig V, Longair M, Pietzsch T, Preibisch S, Rueden C, Saalfeld S, Schmid B, Tinevez J-Y, White DJ, Hartenstein V, Eliceiri K, Tomancak P, Cardona A. Nat Methods 2012;9:676.
[49] Do G, Preuster P, Aslam R, Bösmann A, Müller K, Arlt W, Wasserscheid P. React Chem Eng 2016;1:313.
[50] Peters W, Seidel A, Herzog S, Bösmann A, Schwieger W, Wasserscheid P. Energy Environ Sci 2015;8:3013.
[51] Kadar J, Gackstatter F, Ortner F, Wagner L, Willer M, Preuster P, Wasserscheid P, Geißelbrecht M. Int J Hydrogen Energy 2024;59:1376.